Naturally small Dirac neutrino mass and $B-L$ dark matter

Ernest Ma,[1] Partha Kumar Paul,[2,*] and Narendra Sahu[2,†]

[1]*Department of Physics and Astronomy, University of California, Riverside, California 92521, USA*
[2]*Department of Physics, Indian Institute of Technology Hyderabad, Kandi, Sangareddy, Telangana-502285, India*

(Received 16 January 2026; accepted 4 September 2026; published 23 September 2026)

In the conventional gauged $B-L$ extension of the standard model, the $B-L$ charge of the singlet scalar χ, responsible for the breaking of $U(1)_{B-L}$ symmetry, is taken to be 2, such that it can anchor type-I seesaw by giving Majorana masses to the right-handed neutrinos, ν_R. In this paper, we consider instead the cases $\chi \sim 3$ or 4 under $B-L$, so that ν_R may not acquire any Majorana mass and neutrinos are Dirac fermions. We then consider a vectorlike fermion S with two units of $B-L$ charge, which becomes a good candidate for dark matter, either Dirac for $\chi \sim 3$ or Majorana for $\chi \sim 4$. In both cases, spontaneous $B-L$ breaking can induce a strong first-order phase transition, producing stochastic gravitational waves (GW), which can be tested at GW experiments. Moreover, the presence of light ν_Rs gives rise to an additional contribution to the effective number of relativistic degrees of freedom, $\Delta N_{\rm eff}$, providing complementary constraints from current and upcoming CMB observations.

DOI: 10.1103/386s-sj3r

I. INTRODUCTION

To allow for nonzero neutrino masses, the standard model (SM) of quarks and leptons is routinely extended to include three right-handed neutrinos ν_R. As such, the model accommodates an additional well-known anomaly free $U(1)$ gauge symmetry $B-L$. The spontaneous breaking of $U(1)_{B-L}$ is usually assumed to come from a singlet scalar χ with two units of $B-L$ charge. Hence, ν_R acquires a large Majorana mass, and the type-I seesaw mechanism prevails [1–4]. However, there is a simple alternative. If the $B-L$ charge of $\chi \sim 3$, then a residual global $U(1)$ lepton number remains conserved, and neutrinos are Dirac fermions. This idea was first pointed out [5] in a different context, but it does not explain why these Dirac masses are so small. To do this, we borrow another existing idea, as first pointed out years ago [6]. Assume a $\mathcal{Z}_2$ discrete symmetry, under which ν_R is odd. Add a second Higgs doublet $\eta = (\eta^+, \eta^0)$, which is also odd. Require all dimension-4 terms in the Lagrangian to obey $\mathcal{Z}_2$ but break it softly by the quadratic term $\eta^\dagger \Phi$, where $\Phi = (\phi^+, \phi^0)$ is the SM Higgs doublet. With positive and large μ_η^2 in the scalar potential *i.e.* $\mu_\eta^2 \eta^\dagger \eta$ term, the induced vacuum expectation value $\langle \eta^o \rangle$ is naturally small, thereby guaranteeing small Dirac neutrino masses.[1]

With the introduction of $B-L$ gauge symmetry, an interesting new scenario for dark matter (DM) emerges. Suppose a singlet Dirac fermion $S(=S_L+S_R)$ is added with two units of $B-L$ charge. It has an invariant mass but does not interact with any SM particle except through the $B-L$ gauge boson. Note that the dimension-4 term $\chi \overline{S_L} \nu_R$ is forbidden by $\mathcal{Z}_2$. It is thus stable and is a good candidate for Dirac fermion DM. In this paper, we consider this model, as well as a similar one, where the $B-L$ charge of χ is 4 [9]. If the $B-L$ charge of χ is 4, then it can couple to a vectorlike fermion S as $\chi^\dagger \overline{S^c} S$, where the $B-L$ charge of S is 2. Moreover, S can have a Dirac mass term: $m\overline{S}S$. When χ gets a vacuum expectation value (vev), both S_L and S_R may acquire Majorana masses as well, resulting in two mixed eigenstates, the lighter of which is a candidate for Majorana fermion DM.

We mention in passing that in the canonical choice of $\chi \sim 2$ in the $B-L$ symmetric model, where the Majorana masses of light neutrinos are generated through type-I seesaw, the introduction of a Dirac fermion $S \sim 2$ under $B-L$ also works as dark matter. However, in this case, the dimension-5 $\chi^\dagger \chi^\dagger S_{L,R} S_{L,R}$ terms are admissible, making it only pseudo-Dirac. Other choices of $B-L$ charges for χ and S are also possible for Dirac neutrino mass and dark matter, as can be easily worked out.

*Contact author: ph22resch11012@iith.ac.in
†Contact author: nsahu@phy.iith.ac.in

Published by the American Physical Society under the terms of the Creative Commons Attribution 4.0 International license. Further distribution of this work must maintain attribution to the author(s) and the published article's title, journal citation, and DOI. Funded by SCOAP³.

[1]See Refs. [7,8] for examples of radiative Dirac neutrino mass generation and references therein.

II. DIRAC NEUTRINO MASS AND $\Delta N_{\rm eff}$

The SM gauge group is extended with $U(1)_{B-L}$, which introduces nonzero chiral anomalies. These anomalies get automatically canceled once three right-handed neutrinos (ν_R) are added with $U(1)_{B-L}$ charge -1. An additional $\mathcal{Z}_2$ symmetry is also introduced, under which ν_R is odd, to forbid the $\bar{L}\,\tilde{\Phi}\,\nu_R$ interaction. To forbid Majorana masses of right handed neutrinos, the $B-L$ charge of the singlet scalar χ, responsible for breaking $U(1)_{B-L}$, is given a 3 or 4 charge. These two choices of χ charge lead to two different types of dark matter scenarios, as will be discussed later. To realize the Dirac neutrino mass, one $\mathcal{Z}_2$ odd scalar doublet $\eta = (\eta^+, \eta^0)$ is added with $B-L$ charge of 0. The $\mathcal{Z}_2$ symmetry is softly broken by $\mu_1^2\Phi^\dagger\eta$ interaction, which in turn results in naturally small Dirac neutrino mass. The particles and their charge assignments are shown in Table I. The relevant Yukawa Lagrangian can be written as

$$\mathcal{L}_{\rm Yukawa} = -y_R \bar{L}\,\tilde{\eta}\,\nu_R + \text{H.c.}, \tag{1}$$

The scalar Lagrangian is given as

$$\mathcal{L}_{\rm scalar} = |D_\mu\Phi|^2 + |D_\mu\eta|^2 + |\mathcal{D}_\mu\chi|^2 - V(\Phi,\eta,\chi) + \text{H.c.}, \tag{2}$$

where $D_\mu = \partial_\mu + i\frac{g}{2}\sigma_a W_\mu^a + i\frac{g'}{2}B_\mu$ and $\mathcal{D}_\mu = \partial_\mu + i3(4)g_{\rm BL}(Z_{\rm BL})_\mu$, $g_{\rm BL}$ is the new gauge coupling. The scalar potential is given as

$$\begin{aligned} V(\Phi,\eta,\chi) = {} & -\mu_h^2\Phi^\dagger\Phi + \lambda_h(\Phi^\dagger\Phi)^2 + \mu_\eta^2\eta^\dagger\eta + \lambda_\eta(\eta^\dagger\eta)^2 \\ & - \mu_\chi^2\chi^*\chi + \lambda_\chi(\chi^*\chi)^2 + \lambda_1(\Phi^\dagger\Phi)(\eta^\dagger\eta) \\ & + \lambda_2(\Phi^\dagger\eta)(\eta^\dagger\Phi) + \frac{\lambda_3}{2}[(\Phi^\dagger\eta)^2 + (\eta^\dagger\Phi)^2] \\ & + \mu_1^2\Phi^\dagger\eta + \lambda_{h\chi}(\Phi^\dagger\Phi)(\chi^*\chi) \\ & + \lambda_{\eta\chi}(\eta^\dagger\eta)(\chi^*\chi) + \text{H.c.} \end{aligned} \tag{3}$$

In the effective theory, the scalar fields can be parametrized as

$$\Phi = \begin{pmatrix} 0 \\ \frac{h+v_h}{\sqrt{2}} \end{pmatrix}, \quad \eta = \begin{pmatrix} \eta^+ \\ \frac{\eta_R + v_\eta + i\eta_I}{\sqrt{2}} \end{pmatrix}, \quad \chi = \frac{\chi' + v_\chi}{\sqrt{2}}, \tag{4}$$

TABLE I. Particles and their charge assignments under $U(1)_{B-L}\times\mathcal{Z}_2$ symmetry.

Particles	$U(1)_{B-L}$	$\mathcal{Z}_2$
L	-1	$+$
Φ	0	$+$
ν_R	-1	$-$
η	0	$-$
χ	3(4)	$+$

where v_h, v_η, v_χ are the vevs of Φ, η, and χ, respectively. We note that η acquires an induced vev, $v_\eta \simeq \frac{\mu_1^2 v_h}{\sqrt{2}m_{\eta_R}^2}$, which is naturally small by considering μ_1/m_{η_R} to be small. The η_R and η_I masses are related as $m_{\eta_R}^2 - m_{\eta_I}^2 = \lambda_3 v_h^2$. Assuming $m_{\eta_R} \gg m_h, m_\chi$, we neglect the mixing between $h-\eta$ and $\chi-\eta$. The relevant scalar mixing for our purpose only exists between $h-\chi$. Mass matrix for the CP even states in the basis $(h\chi)$ is

$$\mathcal{M}^2 = \begin{pmatrix} 2\lambda_h v_h^2 & \lambda_{h\chi} v_h v_\chi \\ \lambda_{h\chi} v_h v_\chi & 2\lambda_\chi v_\chi^2 \end{pmatrix}. \tag{5}$$

The mixing angle is given as

$$\tan 2\gamma = \frac{\lambda_{h\chi} v_h v_\chi}{\lambda_\chi v_\chi^2 - \lambda_h v_h^2}. \tag{6}$$

The Dirac neutrino mass can be realized at tree level as shown in Fig. 1. Neutrino mass is given as

$$m_\nu = y_R v_\eta \simeq y_R \frac{1}{m_{\eta_R}^2}\mu_1^2\frac{v_h}{\sqrt{2}}. \tag{7}$$

Assuming $m_\nu \sim 0.05$ eV and $y_R \sim 10^{-4}$, we get $\frac{\mu_1}{m_{\eta_R}} \sim 5\times 10^{-5}$.

In this scenario, the presence of light right-handed neutrinos ν_R can give rise to an additional contribution to the effective number of relativistic degrees of freedom (d.o.f.), $\Delta N_{\rm eff}$. In the absence of these additional light d.o.f., the SM predicts a precise value for the effective number of relativistic species, namely, $N_{\rm eff}^{\rm SM} = 3.045$ [10–12]. Depending on the value of y_R, both thermal and nonthermal production of ν_R can occur. For sufficiently large values of the coupling y_R, the ν_R states can be thermalized through processes such as $\nu_R\nu_L \to \nu_R\nu_L$, $\nu_R\eta^- \to \nu_R\eta^-$, $\nu_R\eta^+ \to \nu_R\eta^+$, and $\nu_R\eta_{R/I} \to \nu_R\eta_{R/I}$. If the interaction rates of these processes fall below the Hubble expansion rate before the decoupling of the SM neutrinos, ν_R and ν_L subsequently evolve with different temperatures. The resulting population of relativistic ν_R then contributes to $\Delta N_{\rm eff}$, as given by [13]

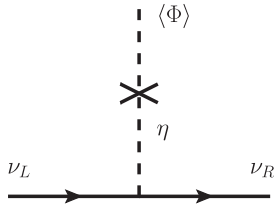


FIG. 1. Tree-level Dirac neutrino mass.

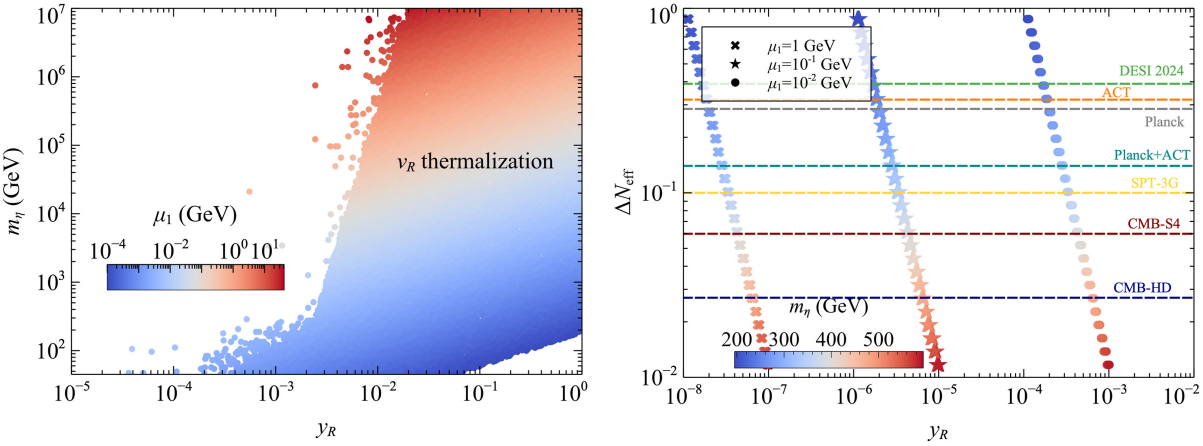


FIG. 2. [*Left*:] parameter space delineating the thermal and non-thermal regions in the m_η–y_R plane. The color code denotes μ_1 values. [*Right*:] $\Delta N_{\rm eff}$ as a function of y_R for three values of μ_1, as indicated in the inset. Constraints from current CMB observations and projected sensitivities of future CMB experiments are shown by different colored dashed lines.

$$\Delta N_{\rm eff} = N_{\rm eff} - N_{\rm eff}^{\rm SM} = N_{\nu_R}\left(\frac{g_{*s}(T^d_{\nu_L})}{g_{*s}(T^d_{\nu_R})}\right)^{\frac{4}{3}}, \tag{8}$$

where the $T^d_{\nu_R}$ is the temperature at which ν_R decouples from the bath and $T^d_{\nu_L}$ is the SM neutrino decoupling temperature which is $\sim$1 MeV, $N_{\nu_R}=3$ is the number of generations of ν_R. In the *left* panel of Fig. 2, we present the region of parameter space in the m_η–y_R plane where ν_R becomes thermalized. The color code represents the values of μ_1. Throughout the $\Delta N_{\rm eff}$ analysis, we fix the neutrino mass scale to $m_\nu = 0.05$ eV using Eq. (7). The colored region corresponds to parameter values for which ν_R is thermalized. In this regime, the resulting contribution to $\Delta N_{\rm eff}$ is always larger than $\sim$0.135 and is therefore excluded by combined Planck + ACT [14]. The white region represents the parameter space where a nonthermal contribution to $\Delta N_{\rm eff}$ arises from the equilibrium decay of η. In this case, the evolution of the energy density of ν_R is governed by the following Boltzmann equation [15,16]:

$$\frac{d\rho_{\nu_R}}{dz} = -\frac{4\beta\nu_R}{z} + \frac{1}{z\mathcal{H}(z)}\langle E\Gamma_\eta\rangle n_\eta^{\rm eq}, \tag{9}$$

where $z = m_\eta/T$, $\beta = 1 + \frac{T}{3g_{*s}(T)}\frac{dg_{*s}}{dT}$, $\langle E\Gamma_\eta\rangle = 2\times 2\frac{m_\eta^2 y_R^2}{32\pi}$, $\mathcal{H}$ is the Hubble expansion rate, and $n_\eta^{\rm eq}$ is the equilibrium number density of η. The $\Delta N_{\rm eff}$ is then computed at CMB epoch as

$$\Delta N_{\rm eff} = N_{\nu_R}\left.\frac{\rho_{\nu_R}}{\rho_{\nu_L}}\right|_{T_{\rm CMB}}, \tag{10}$$

where $\rho_{\nu_L} = 2\frac{7}{8}\frac{\pi^2}{30}T^4$ is the energy density of the SM neutrinos, and $T_{\rm CMB} \simeq 0.26$ eV. In the *right* panel of Fig. 2, we display $\Delta N_{\rm eff}$ as a function of y_R for three different choices of μ_1, as indicated in the inset of the figure. The color coding represents the mass of η. As y_R decreases, the contribution to $\Delta N_{\rm eff}$ correspondingly increases. From this analysis, we find that DESI [17] excludes the region with $m_\eta < 240$ GeV. The Planck [18] data exclude $m_\eta < 260$ GeV. The ACT [14] data exclude $m_\eta < 250$ GeV, while the combined Planck + ACT [14] analysis excludes $m_\eta < 300$ GeV. Future measurements by SPT-3G [19] are expected to exclude $m_\eta < 330$ GeV, CMB-S4 [20] will probe values down to $m_\eta < 380$ GeV, and CMB-HD [21] will be sensitive to regions with $m_\eta < 460$ GeV.

III. FREEZE-OUT RELIC OF DARK MATTER

We assume the reheating temperature of the Universe is much larger than the $U(1)_{B-L}$ symmetry-breaking scale, v_χ. As a result, the DM can be thermally populated because of its $B-L$ gauge interactions. Based on the charge of $U(1)_{B-L}$ symmetry breaking scalar (χ), we consider two separate scenarios: A) DM (S) is a Dirac fermion ($\chi \sim 3$), and B) DM (S) is a Majorana fermion ($\chi \sim 4$).

A. Dirac dark matter

We add a singlet vectorlike fermion, $S(=S_L+S_R)$, with $B-L$ charge of 2. Since the $B-L$ charge of the scalar χ is chosen to be 3, it cannot couple to SS. Also, the dimension-4 term $\chi\overline{S_L}\nu_R$ is forbidden by $\mathcal{Z}_2$. As a result, S behaves as Dirac DM in this scenario. The DM Lagrangian can be written as

$$\mathcal{L}_{\rm DM}^{\rm Dirac} = \bar{S}i\gamma^\mu\mathcal{D}_\mu S - m_S\bar{S}S, \tag{11}$$

where $\mathcal{D}_\mu = \partial_\mu + i2g_{\rm BL}(Z_{\rm BL})_\mu$. The gauge boson, $Z_{\rm BL}$ acquires a mass, $m_{Z_{\rm BL}} = 3g_{\rm BL}v_\chi$ after the breaking of $U(1)_{B-L}$. In this case, the DM S is thermalized through the gauge interactions mediated by $Z_{\rm BL}$. As the temperature

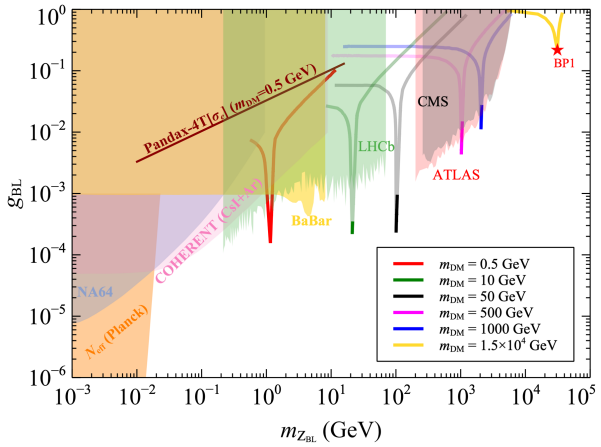


FIG. 3. Correct DM relic parameter space in $g_{\rm BL} - m_{Z_{\rm BL}}$ plane for six choices of DM masses shown with different colored lines. Constraints from CMS [25], ATLAS [26], LHCb [24], NA64 [27], *BABAR* [28], COHERENT [29], $N_{\rm eff}$ (Planck) [30] are shown with different shaded regions.

falls below the mass scale of S, it gets decoupled from the thermal bath, leaving a relic of S.

In this scenario, the free parameters relevant for relic density calculation are $\{m_S \equiv m_{\rm DM}, v_\chi, g_{\rm BL}\}$. The relic density suffers a sharp fall near the $Z_{\rm BL}$ resonance. The DM relic can be satisfied for a large range of DM mass by utilizing the resonance effect. In the Fig. 3, we show the correct relic density parameter space in the plane of $g_{\rm BL}$ vs $m_{Z_{\rm BL}}$ for six different values of DM mass, as shown with different colored lines. The light-colored part of each line is excluded from the direct detection experiment, LZ [22]. The dark-colored part of each line, which is the resonance, is allowed by both the direct detection and relic density constraints. For DM mass of 500 MeV, the constraint from the DM-e scattering experiment PandaX-4T [23] is shown with the dark red solid line. The constraint from LHCb [24] is shown with a green shaded region. The CMS [25] and ATLAS [26] constraints are shown with gray and red shaded regions, respectively. The constraints from NA64 [27], *BABAR* [28], COHERENT [29], and $N_{\rm eff}$ (Planck) [30] are shown with light blue shaded, yellow shaded, and pink shaded regions, respectively.

B. Majorana dark matter

We now turn to the possibility of a Majorana DM. If we extend the Dirac neutrino mass setup with the choice that $B - L$ charge of χ is 4 instead of 3, then the introduction of two chiral fermions S_L and S_R having two units of $B - L$ charges results in Majorana fermion DM. These chiral fermions couple to χ and acquire Majorana masses. They maintain a Dirac mass as well, just as before. On the other hand, ν_R cannot couple to χ or S, so that neutrinos remain Dirac and S is in the dark sector. The dark sector Lagrangian can be written as

$$\mathcal{L}_{\rm DM}^{\rm Majorana} = \overline{S_L} i\gamma^\mu \mathcal{D}_\mu S_L + \overline{S_R} i\gamma^\mu \mathcal{D}_\mu S_R - y_1 \overline{S_L^C} S_L \chi^\dagger - y_2 \overline{S_R^C} S_R \chi^\dagger - m_{12}(\overline{S_R} S_L + \overline{S_L} S_R), \tag{12}$$

We can now write the dark sector mass matrix in the basis $(S_L S_R^C)$ as

$$(\overline{S_L^C}\ \overline{S_R}).\begin{pmatrix} m_L & m_{12} \\ m_{12} & m_R \end{pmatrix}.\begin{pmatrix} S_L \\ S_R^C \end{pmatrix}, \tag{13}$$

where $m_L = \sqrt{2} y_1 v_\chi, m_R = \sqrt{2} y_2 v_\chi$. This mass matrix can be diagonalized with an orthogonal matrix, with a rotation angle given as

$$\tan 2\theta = \frac{2 m_{12}}{m_R - m_L}, \tag{14}$$

resulting in two Majorana mass states S_1, S_2 as $S_i = (S_{iL} + S_{iL}^C)/\sqrt{2}$, where

$$S_{1L} = \cos\theta S_L + \sin\theta S_R^C, \tag{15}$$

$$S_{2L} = -\sin\theta S_L + \cos\theta S_R^C, \tag{16}$$

with masses m_{S_1} and m_{S_2}.

The Yukawa couplings y_1, y_2 and m_{12} can be expressed in terms of physical masses and mixing angle as

$$y_1 = \frac{m_{S_1}\cos^2\theta + m_{S_2}\sin^2\theta}{\sqrt{2} v_\chi}, \tag{17}$$

$$y_2 = \frac{m_{S_2}\cos^2\theta + m_{S_1}\sin^2\theta}{\sqrt{2} v_\chi}, \tag{18}$$

$$m_{12} = \frac{m_{S_2} - m_{S_1}}{2}\sin 2\theta. \tag{19}$$

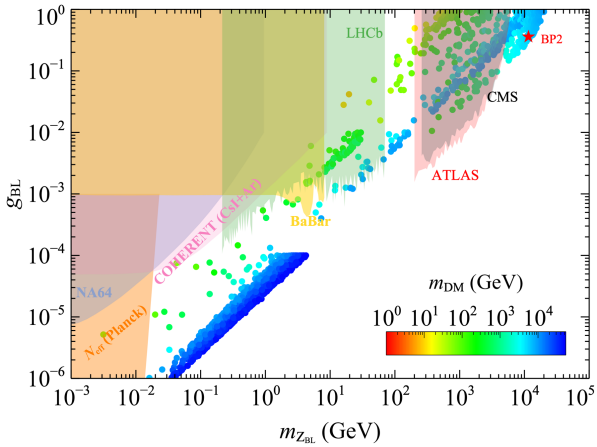


FIG. 4. Correct DM relic parameter space in $g_{\rm BL} - m_{Z_{\rm BL}}$ plane. Constraints from CMS [25], ATLAS [26], LHCb [24], NA64 [27], *BABAR* [28], COHERENT [29], $N_{\rm eff}$ (Planck) [30] are shown with different shaded regions.

TABLE II. Benchmark points giving rise to observable gravitational wave signatures while satisfying constraints from DM relic density, direct detection, and colliders. The BP1 and BP2 are shown with red stars in Figs. 3 and 4, respectively.

BPs	$g_{\rm BL}$	v_χ (GeV)	λ_χ	m_χ (GeV)	$m_{\rm DM}$ (GeV)	T_c (GeV)	T_n (GeV)	T_p (GeV)	$T_{\rm reh}$ (GeV)	α_p	$\beta/\mathcal{H}_p$
BP1	0.217767	47756	0.0035536	4026.09	1.5×10^4	9793.52	2134.87	2024.88	3043.04	0.8063	288.67
BP2	0.358904	8042.41	0.071633	3044.09	5719.44	2915.57	1907.68	1820.76	1854.05	0.0865	253.15

The gauge boson, $Z_{\rm BL}$ acquires a mass, $m_{Z_{\rm BL}} = 4g_{\rm BL}v_\chi$ after the breaking of $U(1)_{B-L}$. The free parameters relevant for relic density calculation are $\{m_{S_1} \equiv m_{\rm DM}, v_\chi, m_\chi, \sin\gamma, g_{\rm BL}\}$. In Fig. 4, we show the points that satisfy both relic density and direct detection constraints in the plane of $g_{\rm BL}$ vs $m_{Z_{\rm BL}}$. The color code denotes the DM mass. Here, we have fixed $m_{S_2} - m_{\rm DM} = 10\,{\rm GeV}$, $\sin\theta = 10^{-2}$. The other parameters are varied as follows: $\{m_{\rm DM} \in [1, 10^5]$ GeV, $g_{\rm BL} \in [10^{-6}, 1]$, $\sin\gamma \in [10^{-4}, 0.7]$, $v_\chi \in [1, 10^5]$ GeV$\}$. In this case, depending on the masses of DM, χ and $Z_{\rm BL}$ the following channels contribute in the relic density determination: $\{S_1S_1 \to ff, \chi\chi, \chi h, hh, \chi Z_{\rm BL}, hZ_{\rm BL}, Z_{\rm BL}Z_{\rm BL}\}$. As expected, with increasing mass of $Z_{\rm BL}$, the cross section decreases, which is compensated by increasing $g_{\rm BL}$. The constraint from LHCb [24] is shown as the green shaded region. Constraints from CMS [25] and ATLAS [26] are depicted by the gray and red shaded regions, respectively. Bounds from NA64 [27], *BABAR* [28], COHERENT [29], and $N_{\rm eff}$ (Planck) [30] are shown as the light blue, yellow, and pink shaded regions, respectively.

IV. GRAVITATIONAL WAVES FROM $U(1)_{B-L}$ SYMMETRY BREAKING

The model also presents intriguing cosmological detection prospects through stochastic gravitational waves, providing a complementary probe of its viability. These gravitational wave signatures originate from the phase transition associated with the spontaneous breaking of $U(1)_{B-L}$. This symmetry is broken when the scalar χ acquires a vev. A first-order phase transition (FOPT) can occur if the true vacuum, where $U(1)_{B-L}$ is broken, has a lower energy density than the high-temperature false vacuum, with a potential barrier separating them. To get the parameter space in which an FOPT occurs, we analyze the structure of the effective potential incorporating the tree-level potential $V_{\rm tree}$, the one-loop Coleman-Weinberg correction $V_{\rm CW}$ [31], and finite-temperature corrections [32,33].

The critical temperature T_c, at which the potential develops two degenerate minima $(0, v_c)$, is determined by studying the temperature evolution of the potential. The ratio v_c/T_c serves as the order parameter, with larger values indicating a stronger first-order phase transition (FOPT). The FOPT proceeds via quantum tunneling, with the tunneling rate estimated by calculating the bounce action S_3. The nucleation temperature T_n is then obtained by equating the tunneling rate per unit volume to the Hubble expansion rate of the Universe, $\Gamma(T_n) = \mathcal{H}^4(T_n)$.

For a strongly supercooled transition (such as BP1), characterized by $T_n/T_c \ll 1$ and $\alpha_n \gg 1$,[2] the standard treatment evaluated at T_n is insufficient. The phase transition does not complete at T_n, it completes at the percolation temperature $T_p < T_n$, defined as the temperature at which enough bubbles of true vacuum have nucleated and grown to fill ∼71% of space. Furthermore, when the bubble network percolates at T_p, the latent heat is released into the plasma, reheating the Universe to the temperature $T_{\rm reh} > T_p$. Since gravitational waves are produced at bubble collision and subsequently redshift from $T_{\rm reh}$, the GW spectrum must be evaluated using the parameters: strength of the transition (α_p) and inverse duration of the transition ($\beta/\mathcal{H}|_{T_p}$) defined at T_p, with $T_{\rm reh}$ as the reference temperature. The details of this analysis are given in Appendix B

We then compute the key parameters required to estimate the stochastic gravitational wave (GW) spectrum originating from bubble collisions [34–38], sound waves in the plasma [39–42], and plasma turbulence [43–48]. The stochastic GW energy density receives contributions from three main sources: bubble wall collisions, sound waves in the plasma, and magnetohydrodynamic turbulence. The total GW spectrum can be expressed as the sum of these individual components,

$$\Omega_{\rm GW}h^2 \approx \Omega_{\rm col}h^2 + \Omega_{\rm sw}h^2 + \Omega_{\rm turb}h^2. \tag{20}$$

We choose two benchmark points for GW from the Dirac DM (BP1) and Majorana DM (BP2) scenarios discussed above. In case of Dirac DM, as there is no interaction between the scalar field χ and the fermion, S, the FOPT is driven by the parameters $\{v_\chi, g_{\rm BL}, \lambda_\chi\}$ only. On the other hand, in the case of Majorana DM, the Majorana fermions interact with χ and modify the Coleman-Weinberg potential. The FOPT sensitive parameters in this case are $\{v_\chi, g_{\rm BL}, \lambda_\chi, y_1, y_2\}$. The parameters are given in Table II. The values of y_1, y_2 corresponding to BP2 are 0.502866 and 0.503746, respectively.

[2] α_n is the strength of the FOPT computed at the nucleation temperature, $\alpha_n = \epsilon(T_n)/\rho_{\rm rad}(T_n)$, ϵ is the latent heat. For the BP1, $\alpha_n = 3.2059$ and for BP2 it is computed to be 0.0741.

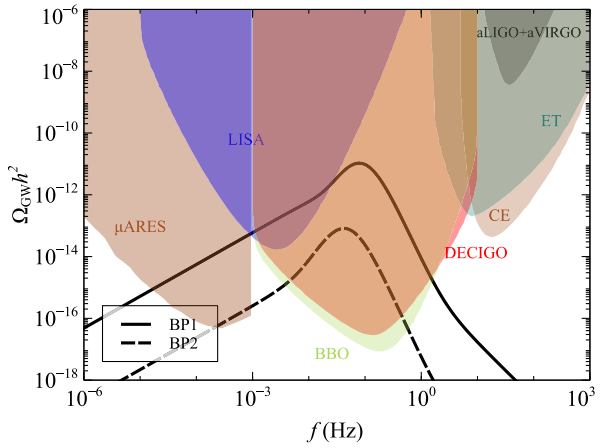


FIG. 5. Gravitational wave spectrum for benchmark points satisfying DM relic as given in Table II.

BP1 is found to be strongly supercooled, with $T_n/T_c = 0.22$ and $\alpha_n = 3.21$, indicating that the vacuum energy dominates over the radiation energy density already at T_n. In this regime, the standard GW analysis evaluated at T_n is insufficient, and a careful percolation analysis is required. We compute the percolation temperature T_p using the full Hubble rate including the vacuum energy contribution as detailed in Appendix B. This yields $T_p = 2024.88$ GeV and, from energy conservation, the reheating temperature $T_{\rm reh} = 3043.04$ GeV. The strength parameter $\alpha_p = 0.8063 < 1$ confirms that at T_p the transition is no longer vacuum dominated, percolation completes successfully. For BP2, with $T_n/T_c = 0.65$ and $\alpha_n = 0.074$, the transition is only mildly supercooled and the corrections are moderate: $T_p = 1820.76$ GeV, $T_{\rm reh} = 1854.05$ GeV, and $\alpha_p = 0.087$.

In Fig. 5, we show the gravitational wave amplitude as a function of frequency for BP1 and BP2 as mentioned in Table II. Sensitivities from LISA [49], DECIGO [50], μARES [51], BBO [52], CE [53], ET [54], aLIGO, aVIRGO [53] are shown with different colored shaded regions. The peak amplitude lies in the sensitivity ranges of LISA, DECIGO, and BBO.

V. CONCLUSIONS

In this paper, we studied a variant of gauged $B-L$ symmetric model where the singlet scalar χ, responsible for breaking the $U(1)_{B-L}$ symmetry, has $B-L$ charge 3 or 4. As a result, the right-handed neutrinos (ν_R with -1 $B-L$ charge) do not acquire any Majorana masses even after the $B-L$ symmetry is broken. If the $B-L$ charge of χ is 3, then we find a possibility of a Dirac fermionic dark matter. On the other hand, if the $B-L$ charge of χ is 4, then the DM can have both Dirac as well as Majorana masses, leading to a pseudo-Dirac DM candidate. In either case, the correct relic density of DM can be achieved through freeze-out of various processes. The model further predicts distinctive cosmological signatures in the form of stochastic gravitational waves generated during the first-order phase transition associated with the breaking of the $U(1)_{B-L}$ symmetry, which can be probed at present and future gravitational wave experiments. In addition, the presence of light right-handed neutrinos in this framework leads to a potentially observable contribution to $\Delta N_{\rm eff}$ through their thermal or nonthermal production in the early Universe. Current and future CMB observations therefore provide a complementary and powerful probe of this scenario, offering an independent test of the Dirac neutrino sector beyond laboratory experiments.

ACKNOWLEDGMENTS

P. K. P. acknowledges the Ministry of Education, Government of India, for providing financial support for his research via the Prime Minister's Research Fellowship (PMRF) scheme.

DATA AVAILABILITY

There are no publicly available research data or software supporting this manuscript. Requests for further information or data should be sent to the authors.

APPENDIX A: FEYNMAN DIAGRAMS RESPONSIBLE FOR THERMALIZATION OF ν_R

In Fig. 6, we present the Feynman diagrams of the processes responsible for maintaining thermal equilibrium among ν_R and the Standard Model bath.

APPENDIX B: DETAILS OF SUPERCOOLED FIRST-ORDER PHASE TRANSITION

The spontaneous breaking of the $U(1)_{B-L}$ symmetry occurs through a first-order phase transition once the scalar χ develops a vacuum expectation value. In the usual approach, the resulting gravitational-wave spectrum is computed at the nucleation temperature T_n, defined as the temperature at which, on average, one bubble nucleates within one Hubble volume during one Hubble time. This treatment, however, becomes unreliable in the strongly supercooled regime, where $T_n/T_c \ll 1$ and $\alpha_n \gg 1$. In such cases, a more refined description of the phase transition is necessary. In this appendix, we briefly describe the improved treatment based on the percolation

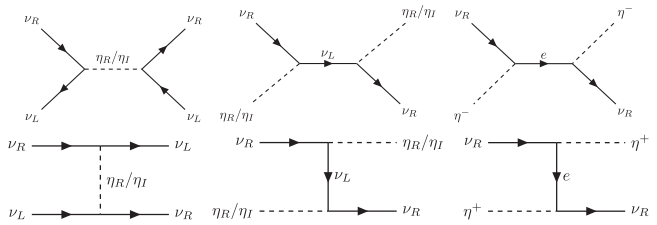


FIG. 6. Diagrams contributing to the thermalization of ν_R.

temperature T_p and the reheating temperature $T_{\rm reh}$, and apply it to both benchmark points in Table II. The thermal nucleation rate of true-vacuum bubbles per unit volume is given by

$$\Gamma = T^4 e^{-S_3/T}\left(\frac{S_3/T}{2\pi}\right)^{3/2}, \tag{B1}$$

where S_3 is the bounce action. The nucleation temperature T_n is then defined by the condition $\Gamma(T_n)/\mathcal{H}(T_n)^4 \sim 1$. While T_n marks the onset of nucleation, it does not describe when the transition actually completes. To quantify this, we compute the average number of bubbles nucleated per unit volume, weighted by their physical volume [55–57],

$$I(T) = \frac{4\pi v_w^3}{3}\int_T^{T_c}\frac{dT'}{T'^4\mathcal{H}(T')}\Gamma(T')\left(\int_T^{T'}\frac{dT''}{\mathcal{H}(T'')}\right)^3, \tag{B2}$$

where $v_w \simeq 1$ is the bubble wall velocity and the Hubble rate $\mathcal{H}$ includes the contribution from the false vacuum energy $\Delta V(T) = V(0,T) - V(v_\chi, T)$ along with the radiation energy density $\rho_{\rm rad}$, which can dominate over the radiation energy density in the supercooled regime and is given as

$$\mathcal{H} = \sqrt{\frac{\rho_{\rm rad}(T) + \Delta V(T)}{3M_{\rm pl}^2}}, \tag{B3}$$

with $M_{\rm pl} = 2.435 \times 10^{18}$ GeV is the reduced Planck mass. The percolation temperature T_p is defined as the temperature at which enough bubbles have nucleated and expanded to fill approximately 71% of space, so that the bubble network percolates, and the transition completes throughout the universe. This condition is expressed in terms of the false vacuum fraction as

$$P_{\rm false}(T_p) = e^{-I(T_p)} \approx 0.71 = e^{-0.34}. \tag{B4}$$

Once percolation completes at T_p, the latent heat stored in the false vacuum, $\Delta V(T_p)$, is rapidly converted into radiation through bubble collisions. This reheats the plasma from T_p to the reheating temperature $T_{\rm reh}$, determined by energy conservation,

$$\rho_{\rm rad}(T_{\rm reh}) = \rho_{\rm rad}(T_p) + \Delta V(T_p). \tag{B5}$$

Since gravitational waves are produced at the moment of bubble collision and subsequently redshifted from $T_{\rm reh}$ when the Universe reenters radiation domination, the GW spectrum must be evaluated using parameters defined at T_p and $T_{\rm reh}$ rather than T_n. The phase transition strength parameter is

$$\alpha_p = \frac{\epsilon(T_p)}{\rho_{\rm rad}(T_{\rm reh})}, \tag{B6}$$

where latent heat ϵ is given as

$$\epsilon(T_p) = \Delta V(T_p) - \frac{T_p}{4}\frac{d\Delta V}{dT}\bigg|_{T_p}, \tag{B7}$$

and the inverse duration of the transition is

$$\frac{\beta}{\mathcal{H}}\bigg|_{T_p} = T_p\frac{d(S_3/T)}{dT}\bigg|_{T_p}. \tag{B8}$$

In Fig. 7, we show $P_{\rm false}(T)$ as a function of temperature for both benchmark points. The red dashed line marks the percolation threshold $P_{\rm false} = e^{-0.34} \approx 0.71$. The vertical green dotted line indicates T_p.

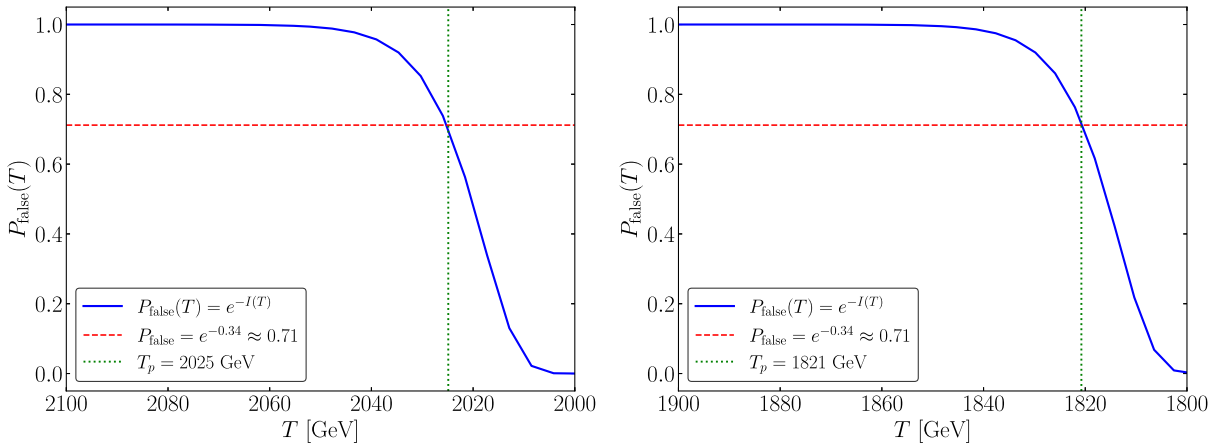


FIG. 7. False vacuum fraction $P_{\rm false}(T) = e^{-I(T)}$ as a function of temperature for BP1 (left) and BP2 (right). The red dashed line marks the percolation threshold $P_{\rm false} = e^{-0.34} \approx 0.71$. The vertical green dotted line indicates T_p.

[1] P. Minkowski, $\mu \to e\gamma$ at a rate of one out of 10^9 muon decays?, Phys. Lett. **67B**, 421 (1977).

[2] M. Gell-Mann, P. Ramond, and R. Slansky, Complex spinors and unified theories, Conf. Proc. C **790927**, 315 (1979).

[3] R. N. Mohapatra and G. Senjanovic, Neutrino mass and spontaneous parity nonconservation, Phys. Rev. Lett. **44**, 912 (1980).

[4] J. Schechter and J. W. F. Valle, Neutrino masses in $SU(2) \times U(1)$ theories, Phys. Rev. D **22**, 2227 (1980).

[5] E. Ma, I. Picek, and B. Radovčić, New scotogenic model of neutrino mass with $U(1)_D$ gauge interaction, Phys. Lett. B **726**, 744 (2013).

[6] E. Ma, Naturally small seesaw neutrino mass with no new physics beyond the TeV scale, Phys. Rev. Lett. **86**, 2502 (2001).

[7] E. Ma and O. Popov, Pathways to naturally small Dirac neutrino masses, Phys. Lett. B **764**, 142 (2017).

[8] A. Dasgupta, S. K. Kang, and O. Popov, Radiative Dirac neutrino mass, neutrinoless quadruple beta decay, and dark matter in $B - L$ extension of the standard model, Phys. Rev. D **100**, 075030 (2019).

[9] J. Heeck and W. Rodejohann, Neutrinoless quadruple beta decay, Europhys. Lett. **103**, 32001 (2013).

[10] G. Mangano, G. Miele, S. Pastor, T. Pinto, O. Pisanti, and P. D. Serpico, Relic neutrino decoupling including flavor oscillations, Nucl. Phys. **B729**, 221 (2005).

[11] E. Grohs, G. M. Fuller, C. T. Kishimoto, M. W. Paris, and A. Vlasenko, Neutrino energy transport in weak decoupling and big bang nucleosynthesis, Phys. Rev. D **93**, 083522 (2016).

[12] P. F. de Salas and S. Pastor, Relic neutrino decoupling with flavour oscillations revisited, J. Cosmol. Astropart. Phys. 07 (2016) 051.

[13] X. Luo, W. Rodejohann, and X.-J. Xu, Dirac neutrinos and $N_{\rm eff}$, J. Cosmol. Astropart. Phys. 06 (2020) 058.

[14] E. Calabrese *et al.* (Atacama Cosmology Telescope Collaboration), The Atacama Cosmology Telescope: DR6 constraints on extended cosmological models, J. Cosmol. Astropart. Phys. 11 (2025) 063.

[15] A. Biswas, D. Borah, N. Das, and D. Nanda, Freeze-in dark matter via a light Dirac neutrino portal, Phys. Rev. D **107**, 015015 (2023).

[16] E. Ma, P. K. Paul, and N. Sahu, Cosmological probes of lepton parity freeze-in dark matter: $\Delta N_{\rm eff}$ & gravitational waves, Nucl. Phys. **B1027**, 117478 (2026).

[17] H. Firouzjahi, and A. Riotto, DESI 2024 VI: Cosmological constraints from the measurements of baryon acoustic oscillations, J. Cosmol. Astropart. Phys. 02 (2024) 021.

[18] N. Aghanim *et al.* (Planck Collaboration), Planck 2018 results. VI. Cosmological parameters, Astron. Astrophys. **641**, A6 (2020); Astron. Astrophys.**652**, C4(E) (2021).

[19] J. S. Avva *et al.* (SPT-3G Collaboration), Particle physics with the cosmic microwave background with SPT-3G, J. Phys. Conf. Ser. **1468**, 012008 (2020).

[20] K. Abazajian *et al.*, CMB-S4 science case, reference design, and project plan, arXiv:1907.04473.

[21] S. Aiola *et al.* (CMB-HD Collaboration), Snowmass2021 CMB-HD white paper, arXiv:2203.05728.

[22] J. Aalbers *et al.* (LZ Collaboration), Dark matter search results from 4.2 tonne-years of exposure of the LUX-ZEPLIN (LZ) experiment, Phys. Rev. Lett. **135**, 011802 (2025).

[23] S. Li *et al.* (PandaX Collaboration), Search for light dark matter with ionization signals in the PandaX-4T experiment, Phys. Rev. Lett. **130**, 261001 (2023).

[24] R. Aaij *et al.* (LHCb Collaboration), Search for $A' \to \mu^+\mu^-$ decays, Phys. Rev. Lett. **124**, 041801 (2020).

[25] A. M. Sirunyan *et al.* (CMS Collaboration), Search for resonant and nonresonant new phenomena in high-mass dilepton final states at $\sqrt{s} = 13$ TeV, J. High Energy Phys. 07 (2021) 208.

[26] G. Aad *et al.* (ATLAS Collaboration), Search for high-mass dilepton resonances using 139 fb^{-1} of pp collision data collected at $\sqrt{s} = 13$ TeV with the ATLAS detector, Phys. Lett. B **796**, 68 (2019).

[27] D. Banerjee *et al.*, Dark matter search in missing energy events with NA64, Phys. Rev. Lett. **123**, 121801 (2019).

[28] J. P. Lees *et al.* (*BABAR* Collaboration), Search for a dark photon in e^+e^- collisions at *BABAR*, Phys. Rev. Lett. **113**, 201801 (2014).

[29] M. Cadeddu, N. Cargioli, F. Dordei, C. Giunti, Y. F. Li, E. Picciau, and Y. Y. Zhang, Constraints on light vector mediators through coherent elastic neutrino nucleus scattering data from COHERENT, J. High Energy Phys. 01 (2020) 116.

[30] D. K. Ghosh, P. Ghosh, S. Jeesun, and R. Srivastava, $N_{\rm eff}$ at CMB challenges U(1)X light gauge boson scenarios, Phys. Rev. D **110**, 075032 (2024).

[31] S. R. Coleman and E. J. Weinberg, Radiative corrections as the origin of spontaneous symmetry breaking, Phys. Rev. D **7**, 1888 (1973).

[32] L. Dolan and R. Jackiw, Symmetry behavior at finite temperature, Phys. Rev. D **9**, 3320 (1974).

[33] M. Quiros, Finite temperature field theory and phase transitions, in *ICTP Summer School in High-Energy Physics and Cosmology* (1999), pp. 187–259, arXiv:hep-ph/9901312.

[34] M. S. Turner and F. Wilczek, Relic gravitational waves and extended inflation, Phys. Rev. Lett. **65**, 3080 (1990).

[35] A. Kosowsky, M. S. Turner, and R. Watkins, Gravitational radiation from colliding vacuum bubbles, Phys. Rev. D **45**, 4514 (1992).

[36] A. Kosowsky, M. S. Turner, and R. Watkins, Gravitational waves from first order cosmological phase transitions, Phys. Rev. Lett. **69**, 2026 (1992).

[37] A. Kosowsky and M. S. Turner, Gravitational radiation from colliding vacuum bubbles: Envelope approximation to many bubble collisions, Phys. Rev. D **47**, 4372 (1993).

[38] M. S. Turner, E. J. Weinberg, and L. M. Widrow, Bubble nucleation in first order inflation and other cosmological phase transitions, Phys. Rev. D **46**, 2384 (1992).

[39] M. Hindmarsh, S. J. Huber, K. Rummukainen, and D. J. Weir, Gravitational waves from the sound of a first order phase transition, Phys. Rev. Lett. **112**, 041301 (2014).

[40] J. T. Giblin and J. B. Mertens, Gravitional radiation from first-order phase transitions in the presence of a fluid, Phys. Rev. D **90**, 023532 (2014).

[41] M. Hindmarsh, S. J. Huber, K. Rummukainen, and D. J. Weir, Numerical simulations of acoustically generated gravitational waves at a first order phase transition, Phys. Rev. D **92**, 123009 (2015).
[42] M. Hindmarsh, S. J. Huber, K. Rummukainen, and D. J. Weir, Shape of the acoustic gravitational wave power spectrum from a first order phase transition, Phys. Rev. D **96**, 103520 (2017); Phys. Rev. D**101**, 089902(E) (2020).
[43] M. Kamionkowski, A. Kosowsky, and M. S. Turner, Gravitational radiation from first order phase transitions, Phys. Rev. D **49**, 2837 (1994).
[44] A. Kosowsky, A. Mack, and T. Kahniashvili, Gravitational radiation from cosmological turbulence, Phys. Rev. D **66**, 024030 (2002).
[45] C. Caprini and R. Durrer, Gravitational waves from stochastic relativistic sources: Primordial turbulence and magnetic fields, Phys. Rev. D **74**, 063521 (2006).
[46] G. Gogoberidze, T. Kahniashvili, and A. Kosowsky, The spectrum of gravitational radiation from primordial turbulence, Phys. Rev. D **76**, 083002 (2007).
[47] C. Caprini, R. Durrer, and G. Servant, The stochastic gravitational wave background from turbulence and magnetic fields generated by a first-order phase transition, J. Cosmol. Astropart. Phys. 12 (**2009**) 024.
[48] P. Niksa, M. Schlederer, and G. Sigl, Gravitational waves produced by compressible MHD turbulence from cosmological phase transitions, Classical Quantum Gravity **35**, 144001 (2018).
[49] P. Amaro-Seoane *et al.* (LISA Collaboration), Laser interferometer space antenna, arXiv:1702.00786.
[50] N. Seto, S. Kawamura, and T. Nakamura, Possibility of direct measurement of the acceleration of the universe using 0.1-Hz band laser interferometer gravitational wave antenna in space, Phys. Rev. Lett. **87**, 221103 (2001).
[51] A. Sesana *et al.*, Unveiling the gravitational universe at μ-Hz frequencies, Exp. Astron. **51**, 1333 (2021).
[52] V. Corbin and N. J. Cornish, Detecting the cosmic gravitational wave background with the big bang observer, Classical Quantum Gravity **23**, 2435 (2006).
[53] B. P. Abbott *et al.* (LIGO Scientific Collaboration), Exploring the sensitivity of next generation gravitational wave detectors, Classical Quantum Gravity **34**, 044001 (2017).
[54] M. Punturo *et al.*, The Einstein Telescope: A third-generation gravitational wave observatory, Classical Quantum Gravity **27**, 194002 (2010).
[55] A. H. Guth and S. H. H. Tye, Phase transitions and magnetic monopole production in the very early universe, Phys. Rev. Lett. **44**, 631 (1980); Phys. Rev. Lett.**44**, 963(E) (1980).
[56] A. H. Guth and E. J. Weinberg, Cosmological consequences of a first order phase transition in the SU(5) grand unified model, Phys. Rev. D **23**, 876 (1981).
[57] J. Ellis, M. Lewicki, J. M. No, and V. Vaskonen, Gravitational wave energy budget in strongly supercooled phase transitions, J. Cosmol. Astropart. Phys. 06 (2019) 024.